Probing Collective Motions of Terminally Anchored Polymers

George Fytas,* Spiros H. Anastasiadis,† Rachid Seghrouchni,
Dimitris Vlassopoulos, Junbai Li,‡ Bradford J. Factor,§
Wolfgang Theobald,‖ Chris Toprakcioglu¶

Polymer chains attached by one end to an impenetrable surface at high coverage exemplify a tethered layer of mesoscopic dimensions. At equilibrium, thermal fluctuations of the segment density profile of the brushlike layer reflect the tethered chain dynamics; the probing of these fluctuations by evanescent-wave dynamic light scattering is reported. By utilizing a set of terminally attached layers with thicknesses (L_0) from 45 to 130 nanometers, it was found that there is a preferred wavelength of order L_0 of these fluctuations with a concurrent slowing down of their thermal decay rate. This technique could open the route for the investigation of the largely unexplored area of polymer surface dynamics.

$\mathbf{W}$hen polymer molecules are selectively attached by one end onto a solid surface at relatively high concentrations, the polymer chains avoid one another by extending away from the surface, forming a "brush" (1, 2). The formation of polymer brushes is of technological importance in colloid stabilization and in modifying bulk surfaces and interfaces for improved adhesion, wetting, and wear properties. Such brushes can be created by synthesizing diblock copolymers, in which one shorter block adsorbs strongly to the surface from a solution and the other longer block extends into the solvent. This stretched configuration of tethered chains is used as a model for a wide variety of confined polymer systems (3). Most theoretical and experimental studies (3–10) have addressed the static structure of brushes, such as the density profile above the surface. Although theoretical predictions have been made of their dynamical structure as well (4, 5, 11, 12), direct relevant experimental observation, although much needed (7), is difficult because of the small size of the brush and its low scattering power.

We have addressed this problem by performing evanescent-wave dynamic light-scattering (EWDLS) measurements of asymmetric poly(ethyleneoxide-*b*-styrene) (PEO-PS) copolymers (Fig. 1). Light is re-

flected from a high-refractive index prism; the polymer is attached at the glass surface at the base of the prism, and the evanescent wave propagates through the polymer brush under conditions of total internal reflection. The evanescent wave is then used as the incident beam in photon correlation spectroscopy (13), which allows fluctuations with wave vector $\mathbf{q}$ to be resolved on time scales from 10^{-7} to 10^3 s. From these measurements, we obtained the time-correlation functions $C(q, t)$ of the scattered-light intensity that reflect concentration fluctuations in the brush. Our results show that long-lived fluctuations have a finite wavelength of order L_0 [$O(L_0)$], where L_0 is the equilibrium thickness of the grafted PS layer. This result resembles that for the interal relaxation mode seen in bulk diblock copolymer solutions (14).

Detailed material and surface characterization is essential for the interpretation of the results. The PEO-PS model system in toluene was selected on account of the extensive information on adsorbed amount, kinetics of adsorption, and segment density profiles obtained from ellipsometry, neutron reflectivity, and surface-balance experiments (9, 10). The characteristics of the PEO-PS diblocks and the brushlike grafted layers are given in Table 1. The brush is formed by the stretched PS block that dangles in solution; the anchoring density is $\sigma = 1/s^2$ (chains nm^{-2}), with s the average interanchor spacing. The volume fractions of the end-adsorbed PS at the solid surface indicate that the PS chains in the layer overlap, which places the solutions in the semidilute regime. The L_0 for the grafted PS monolayer corresponds to a parabolic density profile normal to the surface (1, 10). The adsorption conditions of (9, 10) were reproduced, and a copolymer concentration greater than the threshold value for maximum adsorbance

was used. The adsorption process took place for 12 hours; equilibrium was confirmed by the stability of the scattered intensity. The temperature was held constant at 23°C.

It is also important to verify the operation of the experimental setup (Fig. 1) (15, 16). Adjustment of the total reflection spot on the prism surface and tilting of the incident beam relative to the detected volume grossly affects the duration of the counting times necessary to acquire $C(q, t)$ with good statistics. Furthermore, three control EWDLS experiments were performed: (i) Analysis of the evanescent wave scattering from 100-nm latex particles in water leads to a $C(q, t)$ with the predicted mirror effect (15); the particle diffusion coefficient is (4.2×10^{-8} cm^2 s^{-1}) identical

Foundation for Research and Technology-Hellas, Institute of Electronic Structure and Laser, P.O. Box 1527, 711 10 Heraklion, Crete, Greece.

*To whom correspondence should be addressed. Fax: 30-81-391305.
†Also at University of Crete, Physics Department, 711 03 Heraklion, Crete, Greece.
‡Present address: Max-Planck Institute for Colloid and Surface Research, D-12489 Berlin, Germany.
§Present address: Intel Corp., 5000 West Chandler Boulevard, Chandler, AZ 85226, USA.
‖Present address: IBM Germany, P.O. Box 2540, 55015 Mainz, Germany.
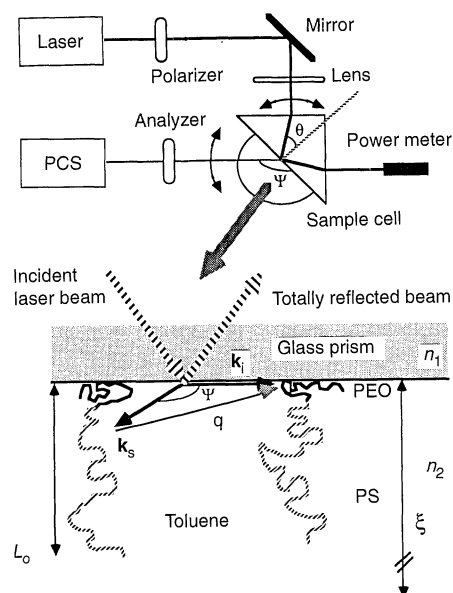¶Also at University of Patras, Physics Department, 265 00 Rio Patras, Greece.

Fig. 1. Schematic diagram of the evanescent wave dynamic light-scattering instrumentation. The light-scattering cell is a right-angle high refractive index ($n_1 = 1.632$) prism to which surface a semicylindrical cell is epoxy-glued. The cell holder is placed on a precision θ-2θ Huber goniometer for independent rotations of the cell relative to the incident laser beam and of the detector arm in order to define both the total reflection angle θ_c, and the various scattering wave vectors $\mathbf{q}$; the detection system is the standard used in conventional photon correlation spectroscopy (13). The enlargement shows the evanescent wave geometry. For total reflection [$\theta > \theta_c = \arcsin(n_2/n_1)$], the evanescent wave propagating parallel to the surface, with an electric field exponentially decaying away from the surface, is scattered by the concentration fluctuations of $\mathbf{q}$[$|\mathbf{q}| = 2k_i\sin(\psi/2)$] in the adsorbed polymer layer; $\mathbf{q} = \mathbf{k}_s - \mathbf{k}_i$, with $\mathbf{k}_i$ and $\mathbf{k}_s$ being the wave vectors of the evanescent and scattered electric field forming a scattering angle ψ. The penetration depth $\xi = (\lambda_0/2\pi n_1)$ $(\sin^2\theta - \sin^2\theta_c)^{-1/2}$, with $\lambda_0 = 488$ nm the light wavelength in vacuum. The critical angle θ_c is determined by measuring the reflected intensity as a function of θ.

to that obtained in bulk solution. (ii) The $C(q, t)$ from PS (weight-averaged molecular weight $M_w = 900$ kg mol^{-1}) solutions in dioxane in the dilute and semidilute regime (0.05 to 1%) reveals the appropriate concentration and q-dependence of the scattered intensity from bulk solutions. (iii) For a dilute solution of PS ($M_w = 1200$ kg mol^{-1}) in toluene (17) (the same solvent as in the PEO-PS layer), $C(q, t)$ exhibits an exponential shape, is insensitive to penetration depth ξ variations (0.4 to 1 μm), and shows a q^2-dependent rate that yields the translational diffusion $D = 9 \times 10^{-8}$ cm^2 s^{-1} in agreement with bulk solution data. The latter are also in agreement with "bulk" measurements obtained in situ for $\theta = \theta_c + 5°$, where the incident light penetrates into the solution as a refracted beam. In fact, such measurements were used in situ to calibrate the scattering angle ψ and hence q in the EWDLS experiment for a given D of the molecule (18). These control experiments show that the standard assertions used in bulk solution measurements are accurate for the present EWDLS. The measured intensity autocorrelation function $G(q, t)$ leads to the computation of the desired $|C(q, t)|^2 = [G(q, t) - A]/f$, where A is the baseline at sufficiently long delay times and f is a coherence (instrumental) factor.

Figure 2 shows $C(q, t)$ for the tethered PS layers. The expected featureless $C(q, t)$ from pure toluene (Fig. 2A) becomes a well-defined decay function after 7 hours of counting for PEO-PS/500 at $q = 0.034$ nm^{-1}. This surface relaxation function clearly reflects dynamics of the grafted layer and not fluctuations due to the translational motion of free polymer chains, which were probed in the control experiment (iii) and measured in the "bulk" geometry (18, 19) (solid line in Fig. 2A). The average scattered intensity I_{tot} is stable over the duration of the EWDLS experiment (inset of Fig. 2A). $C(q, t)$ is well represented by a single exponential function:

$$C(q,t) = a(q)\exp[-\Gamma(q)t] \qquad (1)$$

where $\Gamma(q)$ is the thermal decay rate of the composition fluctuations in the layer. The value of the relaxation amplitude $a(q)$

shows that ~25% of I_{tot} is due to the probed polymer layer mode. Both $C(q, t)$ and the process intensity $I(q) = a(q)I_{tot}$ depend on q (Fig. 2B); $I(q)$ increases with q (inset of Fig. 2B), in support of the homodyne conditions, implying strong suppression of the long-wavelength (low-q) fluctuations, whereas $\Gamma(q)$ for all but the longest PEO-PS chain is virtually insensitive to q (see Fig. 3 below). At comparable qs (0.034 nm^{-1}) and adsorbances A^* (~1.6 mg m^{-2}, Table 1), PEO-PS/500 ($L_0 = 130$ nm) clearly displays a higher $I(q)$ than PEO-PS/150 ($L_0 = 70$ nm), as indicated by the amplitudes of the $C(q, t)$ of Fig. 2C. The intensity data for the four different layers superimpose well when $I(q)$ is divided by A^* and q is normalized to L_0 (inset of Fig. 2C).

On the theoretical side, de Gennes (4, 5) has examined the relaxation processes of physically adsorbed polymers; the lowest relaxation rate for the breathing longitudinal modes was proportional to $q^0 R_F^{-3}/\eta_0$ (R_F, size of the swollen free chain in solution, and η_0, solvent viscosity) and the scattered intensity arising from composition fluctuations at low q's was proportional to $q^2 N^2$.

For a grafted brush, the end-to-end chain relaxation was predicted (11, 12) to depend on N and on the anchoring density σ. Considering mean-squared fluctuations of the chain-free end in the perpendicular direction proportional to L_0^2, a Rouse-like diffusion led to the characteristic q-independent relaxation rate:

$$\Gamma \propto w(\sigma)\sigma^{-\beta}N^{-3} \qquad (2)$$

where $w(\sigma)$ is the microscopic mobility, and $\beta = 2/3$ for free-draining chains or $\beta = 1$ when hydrodynamic interactions were taken into account (12).

Molecular dynamics and Monte Carlo simulations (20–22) were consistent with the scaling prediction of Eq. 2. The simulated chain-end density distribution (21) showed that end monomers were frequently in the outer region of the layer, implying prominent fluctuations with length scale $O(L_0)$. Moreover, fluctuations parallel to the surface were suggested (22) to provide the dominant contribution to the structure factor.

Recently, small-amplitude deformation of the free surface of an incompressible molten "step function" polymer brush was analyzed and the free energy F relative to that of the undeformed flat layer was computed (23–26). Both lateral and perpendicular chain displacements were considered, and the $S(q)$ due to the pair correlation of height fluctuations at the surface exhibited a maximum at a certain value of q^*L_0, because both long- and short-wavelength fluctuations are suppressed for entropic and interfacial tension (γ) costs, respectively. This maximum leads to a preferred wavelength (parallel to the polymer-air interface) $2\pi/q^*$ of the most probable thermally excited surface modes. The value of q^*L_0 depends on
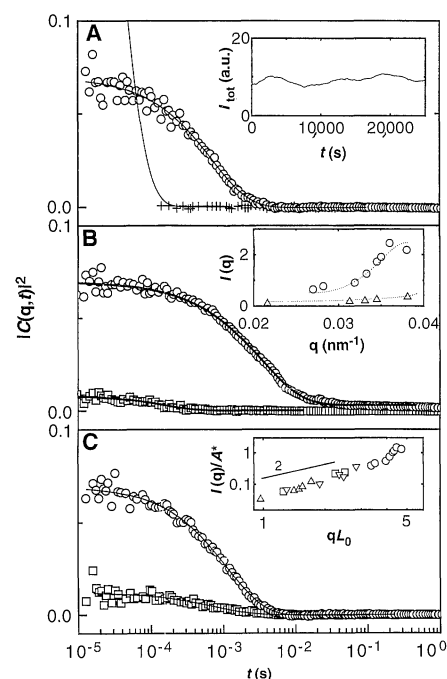

Fig. 2. (A) Correlation functions for the grafted PS layer formed by adsorbing PEO-PS diblock copolymer from toluene solutions at 0.4 mg ml^{-1} and 23°C. The well-defined (O) versus the featureless (+) correlation for the tethered PEO-PS/500 chains at $q = 0.034$ nm^{-1} and for toluene, respectively, and the distinctly different correlation function from the "bulk" solution (solid line) are shown. The profile of the average total scattered intensity corresponding to the end-anchored layer with duration time is depicted in the inset. (B) The dependence of $C(q, t)$ on q (O, 0.034 nm^{-1} and □, 0.022 nm^{-1}) for PEO-PS/500; the inset shows the q dependence of the process intensity $I(q)$ for PEO-PS/500 (O) and PEO-PS/80 (△). (C) Correlation functions for the PEO-PS/500 (O) and PEO-PS/150 (□) specimens at $q = 0.034$ nm^{-1}. The inset depicts the variation of the intensity normalized to the adsorbed mass per area A^* for all four samples with the product qL_0 (△, PEO-PS/80, □, PEO-PS/150, ▽, PEO-PS/184, and O, PEO-PS/500); the data superimpose very well in the regime $qL_0 \approx 1$ to 5. Slope 2 is indicated by the line.

Table 1. Molecular characteristics of the PEO-PS block copolymers (weight-average molecular weight, M_w; number of styrene, N_{PS}, and ethyleneoxide, N_{PEO}, monomer units in the two blocks), adsorbance A^*, and characteristic lengths of the free PS chains and PS layer grafted onto quartz from toluene solution (size of swollen free chain R_F, layer thickness L_0 and the interanchor spacing s) (10).

Sample	M_w (kg mol^{-1})	N_{PS}	N_{PEO}	A^* (mg m^{-2})	R_F (nm)	L_0 (nm)	s (nm)
PEO-PS/80	80	730	90	2.9	14	45 ± 3	7 ± 0.5
PEO-PS/150	150	1420	51	1.6	21	70 ± 5	12 ± 0.5
PEO-PS/184	184	1700	167	2.6	23	80 ± 5	11 ± 0.5
PEO-PS/500	502	4790	91	1.7	42	130 ± 10	23 ± 1

the relative contributions to F at high qs of the γ-term versus that due to chain stretching. The earliest calculation (23) leads to $q^*L_0 \cong 1.44$ for low γ and decreases with increasing γ. Relaxing the assumption that all free chain ends reside at the top layer surface (24) leads to only a slight modification. The assumption that the γ-term dominates at high qs (26), leads to $q^*L_0 \cong 4.6$ for $\gamma = 0.001$ erg cm^{-2}; however, for such γ this assumption fails for our system. A more detailed calculation of F (26) can lead to $q^*L_0 \cong 4.6$ for $\gamma = 0.02$ erg cm^{-2}.

In every case, long-wavelength fluctuations are energetically unfavorable and the height fluctuations are suppressed for $qL_0 \ll 1$, irrespectively of γ. The scattering intensity $I(q)$ at low qL_0 arising from concentration fluctuations can be obtained (27) from the $S(q)$ of height fluctuations (23–26) as:

$$I(q) \propto A^*q^2L_0^2 \qquad (3)$$

where $A^* \propto \sigma N$. The theoretical $(qL_0)^2$ behavior holds for $q/q^* \lesssim 0.5$ (23, 26) or 0.2 (25). The above approaches rely on the assumption that chain trajectories in the brush do not cross.

Although none of these theories have addressed the full structure factor $S(q, t)$ (that is, include its time dependence) they provide the theoretical framework to discuss the experimental results. The evanescent wave is in principle scattered by composition fluctuations throughout the PEO-PS layer swollen with toluene, which has a different refractive index than PS. The

nonuniform distribution of chain ends on the surface appears to emphasize the scattering from surface perturbations. The reduced intensities $I(q)/A^*$ for all layers exhibit a $(qL_0)^2$ dependence at the lower experimental qL_0 range (inset of Fig. 2C), Eq. 3; for the longest PEO-PS/500 layer and at higher qL_0 values, $I(q)$ exhibits a higher rate of increase with q with indications of a broad maximum at the edge of the highest accessible q range; for the other layers, q^* should shift to even higher q's. In order to quantitatively establish the q^* versus L_0 relation and clearly prove the form of $I(q)$, further investigations on brushes with higher L_0 and hence higher N_{PS} would be needed. Nevertheless, the $I(q)$ of PEO-PS/500 suggests that q^*L_0 ($\gtrsim 4.7$) can be reproduced by the recent calculations (23–26).

Because dynamic light scattering in principle probes collective dynamics, $\Gamma(q)$ should bear the thermodynamic effect as expressed in $I(q)$. $\Gamma(q)$ is typically (28) represented by the relation $\Gamma(q) = q^2\Omega g_1(q)/I(q)$, where $g_1(q)$ is the chain form factor and Ω the pure kinetic Onsager coefficient. The distinct drop of $\Gamma(q)$ for PEO-PS/500 at high qs compared to the other samples (Fig. 3) is partly due to the concurrent increase of $I(q)$ (Fig. 2B), and the anticipated $\Omega \propto q^0$ dependence was found. For the thinner layers, the q dependence of $\Gamma(q)$ was compensated from that of $I(q) \propto q^2$ for low qL_0s (Eq. 3); hence, Γ becomes a local relaxation rate (Eq. 2). To reveal the N dependence of Γ, the comparison among the different samples should be made at the same grafting density and local mobility. The $w(\phi) \propto \phi^{-1}$ dependence assumed in the simulation study (21), together with the blob picture of semidilute solutions ($s \approx \phi^{-3/4}$), suggests that $w(\phi) \propto \sigma^{-2/3}$, leading to $\Gamma \propto \sigma^{-b}N^{-3}$ with $b = \beta + 2/3$. The inset of Fig. 3 shows the variation of $\Gamma\sigma^b$ versus N_{PS} for the four layers with $b = 5/3$. The obtained exponent is less than the predicted value of 3 for perpendicular fluctuations (Eq. 2) and increases with increasing contribution of σ.

The equilibrium structure of terminally anchored PS layers (9, 10) conforms to the predictions based on non-uniform chain stretching that yield $L_0 \approx \sigma^{1/3}N$. The study of the dynamic structure of the same system reveals the presence of long-lived thermally induced layer fluctuations with wavelength $2\pi/q^* \cong 1.3L_0$ and indicates strong surface coverage effects on their thermal decay rate. The identification of the precise mechanism of the layer fluctuations would highly benefit from a theoretical calculation of the full structure factor $S(q, t)$ and would promote fundamental studies of polymers near surfaces and provide information on chain relaxation and brush friction, which are relevant to technological applications.
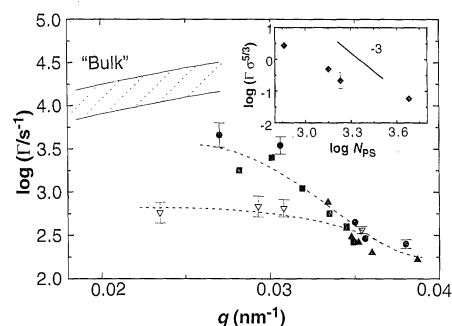
REFERENCES AND NOTES

1. S. T. Milner, *Science* **251**, 905 (1991).
2. R. Yerushalmi-Rozen and J. Klein, *Phys. World* **8**, 30 (August 1995).
3. A. Halperin, M. Tirrell, T. P. Lodge, *Adv. Polym. Sci.* **100**, 31 (1992).
4. P. G. de Gennes, *Adv. Colloid Interface Sci.* **27**, 189 (1987).
5. _____, *C. R. Acad. Sci. Paris Ser. II* **302**, 765 (1986).
6. H. E. Johnson and S. Granick, *Science* **255**, 966 (1992).
7. J. T. Koberstein, Ed., special issue on Polymer Surfaces and Interfaces, *MRS Bull.* **21**, 16–53 (1996).
8. A neutron spin-echo study [B. Farago *et al.*, *Phys. Rev. Lett.* **71**, 1015 (1993)] dealt with the dynamics of density fluctuations of the corona polyisoprene chains in spherical micelles formed by the aggregation of poly(styrene-*b*-isoprene) diblock copolymers in a selective solvent.
9. H. J. Taunton, C. Toprakcioglu, L. J. Fetters, J. Klein, *Macromolecules* **23**, 571 (1990); H. Motschmann, M. Stamm, C. Toprakcioglu, *ibid.* **24**, 3691 (1991).
10. J. B. Field *et al.*, *ibid.* **25**, 434 (1992).
11. A. Halperin and S. Alexander, *Europhys. Lett.* **6**, 329 (1988).
12. L. I. Klushin and A. M. Skvortsov, *Macromolecules* **24**, 1549 (1991).
13. G. Fytas and G. Meier, in *Dynamic Light Scattering. The Method and Some Applications*, W. Brown, Ed. (Oxford Clarendon, London, 1993), pp. 407–436.
14. N. Boudenne *et al.*, *Phys. Rev. Lett.* **77**, 506 (1996); T. Jian *et al.*, *Macromolecules* **27**, 4762 (1994).
15. K. H. Lan, N. Ostrowsky, D. Sornette, *Phys. Rev. Lett.* **57**, 17 (1986).
16. Few attempts to measure dynamic properties of strong scatterers (such as colloidal particles) close to a wall by EWDLS have been reported [(15); see also C. S. Park, M. Copic, R. Mahmood, N. A. Clark, *Liq. Cryst.* **16**, 135 (1995); A. H. Marcus, B. Liu, S. A. Rice, *Phys. Rev. E* **53**, 1965 (1996)]. For weak scattering, however, careful optical alignment to minimize parasitic scattering and control experiments to ensure homodyne detection for both static and dynamic measurements are crucial for the quality of the experimental functions and the technical validity of the data.
17. A PS/toluene solution displays about four times less scattering than an equivalent PS/dioxane solution because of the difference in the refractive index increment.
18. For the PEO-PS samples of Table 1, the translational diffusion coefficients D in dilute toluene solution (0.4 mg ml^{-1}) measured by dynamic light scattering are 4.4×10^{-7}, 3.0×10^{-7}, 3.4×10^{-7}, and 2.0×10^{-7} cm^2 s^{-1} at 23°C, respectively.
19. The possibility of additional contributions due to the translational diffusion of the free polymer chains in the dilute PEO-PS solution in contact to the layer as well as from the collective motion of overlapping tethered PS chains in the layer should be considered. The former should, in principle, be observed if the penetration depth ξ is longer than the layer thickness L_0; its detection depends on the concentration of the free polymer chains and the diffusive translational rate Dq^2 (18). The latter contribution is predicted (4) to have a diffusive character as well with a relaxation rate $D_{coop}q^2$, where the cooperative diffusion $D_{coop} = kT/(6\pi\eta_0 s)$ (kT is the thermal energy, and η_0 the solvent viscosity) in the present layers should assume values similar to D (if we use the interanchor spacing s of Table 1, D_{coop} is computed as 5.4×10^{-7}, 3.3×10^{-7}, 3.6×10^{-7}, and 1.7×10^{-7} cm^2 s^{-1}, respectively). For the shortest PEO-PS/80 layer, $C(q, t)$ at high q's shows an additional faster process that, in contrast to the layer relaxation, is diffusive. Hence, the two processes tend to merge at low q's (see Fig. 3); this, in addition to the decreasing intensity of the layer relaxation with decreasing q (insets of Fig. 2, B and C), renders the analysis of $C(q, t)$ at low q's ambiguous.
20. M. Murat and G. S. Grest, *Macromolecules* **22**, 4054 (1989).
21. P. Y. Lai and K. Binder, *J. Chem. Phys.* **95**, 9288 (1991).
22. J. F. Marko and A. Chakrabarti, *Phys. Rev. E* **48**, 2739 (1993).

Fig. 3. The thermal relaxation rate Γ (Eq. 1) as a function of q for PEO-PS/184 ($\triangledown$) and for three independently prepared layers of PEO-PS/500 ($\bullet$, $\blacktriangle$, and $\blacksquare$). Dashed lines are drawn to guide the eye. The solid lines indicate the upper (for PEO-PS/80) and lower (for PEO-PS/500) limit of the diffusive relaxation rates in the "bulk" solutions and demonstrate the distinctly different dynamics from the end-adsorbed layer. The inset depicts the scaling of $\Gamma\sigma^b$ ($b = 5/3$) at $q = 0.03$ nm^{-1} with molecular weight of the tethered PS chains, implied by Eq. 2 and an effective local mobility (Γ in reciprocal seconds and σ in reciprocal nanometers squared); the predicted slope of -3 is also indicated.

23. G. H. Fredrickson, A. Ajdari, L. Leibler, J. P. Carton, *Macromolecules* **25**, 2882 (1992).
24. H. W. Xi and S. T. Milner, *ibid.* **29**, 4772 (1996).
25. F. J. Solis and G. T. Pickett, *ibid.* **28**, 4307 (1995).
26. D. Long, A. Ajdari, L. Leibler, *Langmuir* **12**, 1675 (1996).
27. By volume conservation ($L = \sigma \nu N$, ν is the monomer volume), $\langle \phi_q^2 \rangle \propto \sigma^2 \langle L_q^2 \rangle$ where ϕ_q and L_q are, respectively, the concentration and layer height fluctuations.
28. R. Kubo, M. Toda, N. Hashitsume, *Statistical Physics II: Nonequilibrium Statistical Mechanics* (Springer, Berlin, 1985).
29. We thank G. Petekidis for his assistance and constructive comments, A. N. Semenov for critically reading the manuscript, and M. Stamm for stimulating discussions. Part of this research was sponsored by the European Union (International Scientific Cooperation, contract ISC*CT93-0951) and by NATO's Scientific Affairs Division (Science for Stability Programme). B.F. acknowledges the support of an NSF/NATO postdoctoral fellowship.

Copper-Catalyzed Oxidation of Alcohols to Aldehydes and Ketones: An Efficient, Aerobic Alternative

István E. Markó,* Paul R. Giles, Masao Tsukazaki, Stephen M. Brown, Chistopher J. Urch

An efficient, copper-based catalyst has been discovered that oxidizes a wide range of alcohols into aldehydes and ketones under mild conditions. This catalytic system utilizes oxygen or air as the ultimate, stoichiometric oxidant, producing water as the only by-product.

The oxidation of alcohols into aldehydes and ketones is a ubiquitous transformation in organic chemistry, and numerous oxidizing agents are available to effect this key reaction (1). In most instances, these reagents are required in stoichiometric amounts and are usually toxic, or hazardous, or both. Moreover, purification of the reaction products is often demanding and laborious. Despite the industrial importance of this process and the ever-growing environmental concerns, surprisingly few efficient catalytic oxidations of alcohols have been described (2). The scarcity of alcohol oxidation processes that simply use oxygen or air as the ultimate stoichiometric oxidant is particularly notable (3, 4).

We describe an efficient, aerobic catalytic system for the transformation of alcohols into carbonyl compounds under mild conditions. Our work was inspired by the seminal report of Jallabert and Rivière and co-workers (5) on the aerobic oxidation of benzylic alcohols mediated by copper-amine complexes (6, 7). This method, however expedient, unfortunately requires 2 equivalents (equiv) of copper complex per equivalent of alcohol. Moreover, it is severely limited in scope to some benzylic alcohol substrates.

I. E. Markó, P. R. Giles, M. Tsukazaki, Université Catholique de Louvain, Département de Chimie, Laboratoire de Chimie Organique, Bâtiment Lavoisier, Place Louis Pasteur 1, B-1348 Louvain-la-Neuve, Belgium.
S. M. Brown, Zeneca Process Technology Department Huddersfield Works, P.O.Box A38, Leeds Road, Huddersfield HD2 1FF, United Kingdom.
C. J. Urch, Zeneca Agrochemicals, Jealott's Hill Research Station, Bracknell, Berkshire RG42 6ET, United Kingdom.

*To whom correspondence should be addressed.

Initial investigations of the effect of various additives on promoting catalyst turnover led to a remarkable result. Substituted azo compounds, such as diethylazodicarboxylate (DEAD) or its *tert*-butyl (Bu^t) analog (DBAD) strikingly improve not only the turnover and the lifetime of the catalyst but also the rate of the reaction (8). The corresponding hydrazines, DEADH$_2$ and DBADH$_2$, are even more competent co-additives.

Further studies showed that the nature of the copper counterion is critical to the success of the reaction, with chloride, acetate, and triflate proving to be the most effective. Among a variety of ligands tested, diamines such as phenanthroline (phen) and its derivatives are particularly efficient. Whereas polar solvents (such as acetonitrile) inhibit the reaction, smooth aerobic oxidation takes place in apolar solvents such as benzene. More significant from a practical viewpoint, toluene and trifluoromethylbenzene are superior solvents to benzene and lead to an important increase in reaction rates (9).
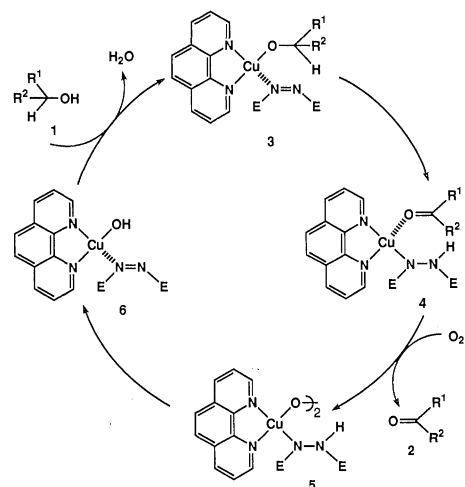
Under the following conditions (5% CuCl, 5% phen, 5% DBADH$_2$, 2 equiv K$_2$CO$_3$, O$_2$ or air, toluene, 70° to 90°C), a wide range of primary, secondary, allylic, and

$$R^2\text{---}\overset{R^1}{\underset{H}{\text{C}}}\text{---OH} \quad \xrightarrow[\substack{5\% \text{ DBADH}_2;\ O_2 \\ \text{Toluene; } 70° \text{ to } 90° \text{ C}}]{\substack{5\% \text{ CuCl; } 5\% \text{ Phen;} \\ 2 \text{ equiv. } K_2CO_3;}} \quad R^2\overset{R^1}{\underset{}{\text{C}}}{=}O$$
1   **2**

benzylic alcohols can be smoothly oxidized to the corresponding aldehydes or ketones in good to excellent yields (Table 1).

Air can be conveniently used instead of oxygen without affecting the efficiency of the process. However, the use of air requires slightly longer reaction times. With activated allylic and benzylic alcohols, lower catalyst loading can be used with only a marginal drop in reaction rate (10). In these cases, lower temperatures can also be applied but result in a longer reaction period. Remarkably, catalyst deactivation is not observed during these extended reaction times (11).

The catalyst shows excellent tolerance for a broad range of alcohol substrates and is notably not deactivated by nitrogen- and sulfur-containing compounds. Sensitive aldehydes, such as neral and geranial, are not isomerized under the reaction conditions.

The active catalyst appears to be heterogeneous and adsorbed on the insoluble K$_2$CO$_3$ (12). Besides its role as a solid support, the carbonate also acts as a base (13), initiating the addition of the alcohol, or DBADH$_2$, or both to the copper complex, and as a water scavenger (14). In several instances, K$_2$CO$_3$ could be replaced by 4 Å molecular sieves and a catalytic amount of a nonoxidizable base such as KOH or KOBu^t.
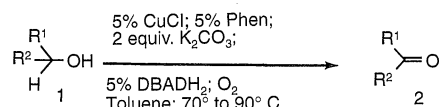
Mechanistic studies suggest that an initial hydrogen-transfer reaction within the copper-alkoxide/azo complex **3** generates the carbonyl-bound hydrazino-copper species **4** (Scheme 1) (15). Upon reaction with oxygen, this copper(I) complex then produces the binuclear copper(II) peroxide **5** (16). Homolytic cleavage followed by hydrogen-atom abstraction from the complexed hydrazine affords the hydroxy Cu(I) species **6**. Rapid exchange between the OH ligand and alcohol **1**, with concomitant loss of a water molecule, regenerates the loaded catalyst **3** and initiates a second catalytic cycle.

Scheme 1. R^1;R^2 = alkyl, aryl, heteroaryl, H; E = COOEt, COOBu^t

We have discovered an efficient catalytic system that oxidizes a wide range of alcohols into the corresponding carbonyl compounds under mild conditions and that uses O$_2$ or